Quadrotor UAV flight control via a novel saturation integral backstepping controller

Laihong Zhou, Juqian Zhang, Houxin She & Hong Jin

Taylor & Francis
Taylor & Francis Group

Quadrotor UAV flight control via a novel saturation integral backstepping controller

Laihong Zhou [a], Juqian Zhang[a], Houxin She[a] and Hong Jin[b]

[a]School of Mechanical Engineering and Automation, Northeastern University, Shenyang, Liaoning, People's Republic of China; [b]School of New Energy Science and Engineering, Xinyu University, Xinyu, Jiangxi, People's Republic of China

ABSTRACT

In this paper, in order to reduce the influence on quadrotor flight from different external disturbances, a novel nonlinear robust controller is designed and used in the quadrotor system. At first, a nonlinear dynamic model of the quadrotor is formulated mathematically. Then, a quadrotor flight controller is designed with the method of classical backstepping control (CBC) and the nonlinear system using this controller is proved to be asymptotically stabilized by the Lyapunov stability theory when there is no external disturbance. At last, a new nonlinear robust controller established by the introduction of both the saturation function and the integral of error into CBC is designed and named as saturation integral backstepping control (SIBC). The boundedness of the nonlinear system under external disturbances is verified by the uniformly ultimately bounded theorem of the nonvanishing perturbation. The numerical simulations of hovering and trajectory tracking are carried out using MATLAB/SIMULINK taking the external disturbances into consideration. In addition, a series of outdoor flight experiments were completed on the actual experimental equipments of quadrotor UAV under the time-varying disturbance from wind. According to the simulation and flight experiment results, the proposed SIBC strategy shows a superior robustness than CBC and integral backstepping control (IBC) strategy.

1. Introduction

As a new kind of small unmanned aerial vehicle (UAV), quadrotor aircraft has been widely concerned and used in military surveillance, rescue, disaster monitoring, photography and agricultural mapping due to its many advantages such as flight by high maneuverability and agility, hovering, vertical take-off and landing, etc. [1–3]. Despite the advantages of quadrotor compared to helicopter in terms of efficiency, dimensional flexibility, smaller spacial requirement and safety, its application has been greatly hindered owing to the complicated flight control design of the quadrotor, for it is an underactuated system with six outputs and only four control inputs [4,5]. In addition, the quadrotor system has high nonlinear, strongly coupled, multivariable, time-varying nature and can be easily affected by external disturbances. Therefore, a control strategy with excellent disturbance restraining capability is urgently required to achieve autonomous flight such as hovering, trajectory tracking, take-off and landing [6].

In order to solve the quadrotor UAV control problem, many new control methods have been proposed by researchers, for example, linear and adaptive proportional–integral–derivative (PID) control [7], fuzzy integral sliding mode control [8], feedback linearization control [9,10], integral predictive/nonlinear H_{∞} control [6], adaptive dynamic feedback-linearization control [11], sliding mode reconfigurable control [12], sliding mode control driven by sliding mode disturbance observer [13], linear matrix inequality (LMI) based robust quadrotor control [14], and robust adaptive attitude tracking control [15,16].

As a regressive design method, the backstepping control is commonly used in nonlinear control methods, because of its superior advantages such as better design flexibility and higher stability compared to other control methods. Based on Lyapunov stability theory, the backstepping control can combine controllers design with Lyapunov function selection perfectly, with the design process for controllers equaling the process of stability proof. Thus, the system can keep asymptotic stability by choosing a Lyapunov function reasonably. However, since the classical backstepping control (CBC) method could hardly resist the external disturbances, many improvements have been done to enhance the capability of resisting disturbance for the backstepping control. For example, to solve the trajectory tracking problem, an adaptive control algorithm is derived based on backstepping [17]. A new approach for the attitude control of a quadrotor aircraft is proposed by combining the backstepping technique and a

CONTACT Hong Jin ✉ jh_syau@126.com 🖳 School of New Energy Science and Engineering, Xinyu University, Xinyu, Jiangxi 338004, People's Republic of China

nonlinear robust proportional integral (PI) controller [18]. Enhanced backstepping controller based on proportional derivative (PD) control is obtained, in which particle swarm optimization (PSO) algorithm has been utilized to determine the controller parameters [19].

Although, the disturbance restraining capability for the backstepping control has been proved to be improved to a certain extent under one kind of external disturbance in the previous reports, the different effects on quadrotor flight between various external disturbances have not been studied, and the proof for the uniformly ultimately boundedness of quadrotor control system in the nonvanishing perturbation condition was almost ignored. Therefore, in this work, three kinds of external disturbances (constant disturbance, periodic disturbance and random disturbance) have been taken into consideration separately during the flight control of quadrotor. In order to reduce the influence of these disturbances to the quadrotor flight (such as hovering and trajectory tracking), a novel saturation integral backstepping control (SIBC) has been proposed by combining saturation function and integral of error with the CBC. In addition, the boundedness of the nonlinear system is verified by the uniformly ultimately bounded theorem of the nonvanishing perturbation. Simulation and flight experiment results indicate that compared with CBC and integral backstepping control (IBC), SIBC strategy shows higher anti-disturbance capacity to the three disturbances in hovering and trajectory tracking respectively.

This paper is organized as follows: a detailed dynamics model of the quadrotor is presented in Section 2. Classical backstepping control is described in Section 3. A saturation proportional integral backstepping controller and the proof of uniformly ultimately boundedness for the system are proposed in Section 4. The simulation results of two cases (hovering and trajectory tracking) are presented in Section 5. The outdoor flight experiments of the quadrotor are given in Section 6. Conclusions are presented in Section 7.

2. Quadrotor dynamics model descriptions

2.1. Control principle

The quadrotor is an underactuated system because it has six degrees of freedom but only four inputs. Each input has one rotor to generate the propeller forces. As shown in Figure 1, the four rotors were recorded as rotor 1, 2, 3 and 4. By varying the speed of the four motors, the quadrotor can produce three attitudes, namely pitch, roll and yaw. The altitude of the vehicle will be changed by varying the four rotor speeds with the same quantity. In order to keep balance or produce yaw motion, two pairs of rotors (rotor 1, 3 and rotor 2, 4) should rotate in two different directions, respectively. Roll motion is produced when the speed of rotor
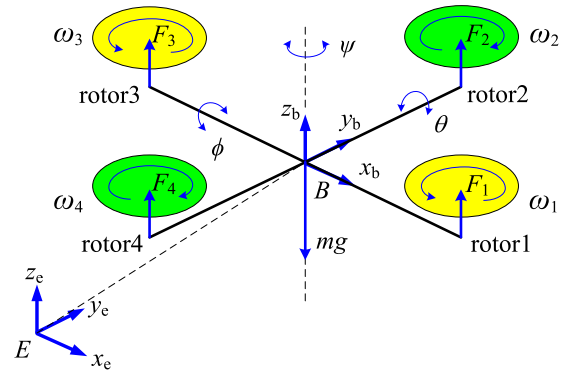
Figure 1. Configuration frame scheme of quadrotor UAV.
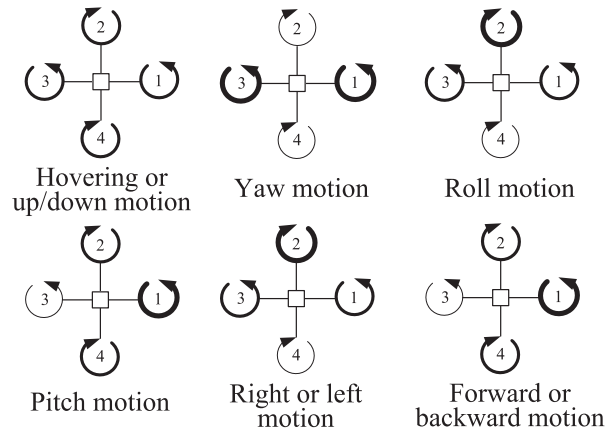
Figure 2. Schematic illustration of motions for quadrotor UAV.

2 is different from that of rotor 4. Similarly, when the speed of rotor 1 is different from that of rotor 3, pitch motion will be produced. The flight mechanisms of the quadrotor are shown in Figure 2.

In order to simplify the modelling, a few assumptions are made first as follows [20,21]:

Assumption 1. The body of the quadrotor system is rigid and strictly symmetrical.

Assumption 2. The body fixed frame origin coincides exactly with the centre of mass.

Assumption 3. There is no blade flapping for the propellers.

Assumption 4. The Euler angles are bounded as $-(\pi/2) < \phi < (\pi/2)$, $-(\pi/2) < \theta < (\pi/2)$ and $-\pi < \psi < \pi$.

2.2. Dynamic model

An earth fixed frame $E(x_e, y_e, z_e)$ and a body fixed frame $B(x_b, y_b, z_b)$ are used to study the system motion of quadrotor. The absolute position of the vehicle and the three Euler angles (roll, pitch and yaw) are described by $\xi = [x, y, z]^T$ and $\eta = [\phi, \theta, \psi]^T$ respectively in earth fixed frame E. The roll angle (ϕ) rotation around x_b-axis, the pitch angle (θ) rotation around y_b-axis and

the yaw angle (ψ) rotation around z_b-axis are shown in Figure 1. The linear velocity is denoted as $V = [u, v, w]^T$ and the angular velocity of the airframe as $\Omega = [p, q, r]^T$ in the body fixed frame B [22,23]. The relation between the body fixed frame velocity and the earth fixed frame velocity can be written as [19,20]

$$\begin{cases} \dot{\xi} = RV \\ \dot{\eta} = N\Omega \end{cases} \tag{1}$$

where R and N are the translation and rotation matrices, and they are given as below:

$$R = \begin{pmatrix} C_\psi C_\theta & C_\psi S_\theta S_\phi - S_\psi C_\phi & C_\psi S_\theta C_\phi + S_\psi S_\phi \\ S_\psi C_\theta & S_\psi S_\theta S_\phi + C_\psi C_\phi & S_\psi S_\theta C_\phi - C_\psi S_\phi \\ -S_\theta & C_\theta S_\phi & C_\theta C_\phi \end{pmatrix} \tag{2}$$

$$N = \begin{pmatrix} 1 & S_\phi T_\theta & C_\phi T_\theta \\ 0 & C_\phi & -S_\phi \\ 0 & S_\phi/C_\theta & C_\phi/C_\theta \end{pmatrix} \tag{3}$$

where the abbreviations $S_{(\cdot)}$, $C_{(\cdot)}$ and $T_{(\cdot)}$ denote $\sin(\cdot)$, $\cos(\cdot)$ and $\tan(\cdot)$, respectively.

Using the Newton-Euler approach, the translational and rotational dynamic equations of motions can be written as follows:

$$\begin{cases} m\ddot{\xi} = F_f + F_d + F_g \\ I\dot{\Omega} + \Omega \times I\Omega = M_f - M_d \end{cases} \tag{4}$$

where $F_f = R\begin{bmatrix} 0 & 0 & \sum_{i=1}^{4} F_i \end{bmatrix}^T$ with $F_i = b\omega_i^2$, F_i and ω_i as the thrust force and speed of the rotor i respectively, b as the thrust factor, $F_d = k_d\dot{\xi} = diag\left(-k_{dx} \quad -k_{dy} \quad -k_{dz}\right)\dot{\xi}$ and $F_g = \begin{bmatrix} 0 & 0 & -mg \end{bmatrix}^T$ are the aerodynamic drag force and the gravitational force, respectively. $\Omega \times I\Omega$ is the gyroscopic effect due to rigid body rotation, while $I = \begin{bmatrix} I_x & I_y & I_z \end{bmatrix}^T$ is the inertia matrix, M_f and $M_d = k_{dm}\Omega = \begin{bmatrix} k_{dmx}p & k_{dmy}q & k_{dmz}r \end{bmatrix}^T$ are torques produced by the propeller system torque and the aerodynamic torque, respectively, k_{dx}, k_{dy}, k_{dz}, k_{dmx}, k_{dmy} and k_{dmz} are drag coefficients, M_f is given as

$$M_f = \begin{bmatrix} lb(\omega_4^2 - \omega_2^2) \\ lb(\omega_3^2 - \omega_1^2) \\ d(\omega_1^2 + \omega_3^2 - \omega_2^2 - \omega_4^2) \end{bmatrix} \tag{5}$$

where l and d are the distance from the rotors to the centre of mass and the drag factor, respectively.

Then, the final dynamic model of quadrotor can be formulated as

$$\begin{bmatrix} \ddot{z} \\ \ddot{\phi} \\ \ddot{\theta} \\ \ddot{\psi} \\ \ddot{x} \\ \ddot{y} \end{bmatrix} = \begin{bmatrix} (C_\theta C_\phi)\frac{1}{m}U_1 \\ \dot{\theta}\dot{\psi}\left(\frac{I_y - I_z}{I_x}\right) \\ \dot{\phi}\dot{\psi}\left(\frac{I_z - I_x}{I_y}\right) \\ \dot{\theta}\dot{\phi}\left(\frac{I_x - I_y}{I_z}\right) \\ (C_\phi C_\psi S_\theta + S_\phi S_\psi)\frac{1}{m}U_1 \\ (C_\phi S_\theta S_\psi - C_\psi S_\phi)\frac{1}{m}U_1 \end{bmatrix} + \begin{bmatrix} -\frac{k_{dz}}{m}\dot{z} \\ \frac{l}{I_x}U_2 \\ \frac{l}{I_y}U_3 \\ \frac{1}{I_z}U_4 \\ -\frac{k_{dx}}{m}\dot{x} \\ -\frac{k_{dy}}{m}\dot{y} \end{bmatrix}$$

$$+ \begin{bmatrix} -g \\ -\frac{k_{dmx}}{I_x}\dot{\phi} - \frac{J_r}{I_x}\dot{\theta}\omega_r \\ -\frac{k_{dmy}}{I_y}\dot{\theta} + \frac{J_r}{I_y}\dot{\phi}\omega_r \\ -\frac{k_{dmz}}{I_z}\dot{\psi} \\ 0 \\ 0 \end{bmatrix} \tag{6}$$

where J_r is the rotor inertia and $\omega_r = \omega_2 + \omega_4 - \omega_1 - \omega_3$. The control inputs are given as

$$\begin{cases} U_1 = b(\omega_1^2 + \omega_2^2 + \omega_3^2 + \omega_4^2) \\ U_2 = b(\omega_4^2 - \omega_2^2) \\ U_3 = b(\omega_3^2 - \omega_1^2) \\ U_4 = d(\omega_1^2 + \omega_3^2 - \omega_2^2 - \omega_4^2) \end{cases} \tag{7}$$

3. Classical backstepping control for the quadrotor UAV

Because the quadrotor UAV at a low speed, in this section, the aerodynamic drag force F_d and the aerodynamic torque M_d are ignored, while the external disturbance is not taken into account either. The nonlinear dynamic equation is described as [19]

$$\ddot{X} = f(X) + g(X)U \tag{8}$$

where the state vector and input vector are given as below:

$$X = \begin{bmatrix} x_1 & x_2 & x_3 & x_4 & x_5 & x_6 \end{bmatrix}^T$$
$$= \begin{bmatrix} z & \phi & \theta & \psi & x & y \end{bmatrix}^T \tag{9}$$
$$U = \begin{bmatrix} U_1 & U_2 & U_3 & U_4 \end{bmatrix}^T \tag{10}$$

The two virtual control inputs are defined as follows:

$$\begin{cases} u_x = C_\phi C_\psi S_\theta + S_\phi S_\psi \\ u_y = C_\phi S_\theta S_\psi - C_\psi S_\phi \end{cases} \tag{11}$$

The dynamics model (6) can be rewritten as follows:

$$\ddot{X} = f(X) + g(X)U = \begin{bmatrix} -g \\ a_1\dot{x}_3\dot{x}_4 + a_2\omega_r\dot{x}_3 \\ a_3\dot{x}_2\dot{x}_4 + a_4\omega_r\dot{x}_2 \\ a_5\dot{x}_2\dot{x}_3 \\ 0 \\ 0 \end{bmatrix}$$

$$+ \begin{bmatrix} \frac{1}{m}C_\phi C_\theta & 0 & 0 & 0 \\ 0 & b_1 & 0 & 0 \\ 0 & 0 & b_2 & 0 \\ 0 & 0 & 0 & b_3 \\ \frac{1}{m}u_x & 0 & 0 & 0 \\ \frac{1}{m}u_y & 0 & 0 & 0 \end{bmatrix} U \qquad (12)$$

x_{ij} $(i = 1, 2 \ldots 6, j = 1, 2 \ldots 4)$ is an element of $g(\boldsymbol{X})$ and the abbreviations are given below:

$$\begin{cases} a_1 = (I_y - I_z)/I_x \\ a_2 = -J_r/I_x \\ a_3 = (I_z - I_x)/I_y \\ a_4 = J_r/I_y \\ a_5 = (I_x - I_y)/I_z \end{cases} \quad \begin{cases} b_1 = l/I_x \\ b_2 = l/I_y \\ b_3 = 1/I_z \end{cases} \qquad (13)$$

The state trajectory of quadrotor can track a desired reference trajectory $\boldsymbol{X_d} = \begin{bmatrix} x_{1d} & x_{2d} & x_{3d} & x_{4d} & x_{5d} & x_{6d} \end{bmatrix}^T = \begin{bmatrix} z_d & \phi_d & \theta_d & \psi_d & x_d & y_d \end{bmatrix}^T$ without external disturbance by using a suitable control law which was obtained with the CBC method. Take the control input U_1 for example, the design of CBC is given step-by-step as follows:

Step 1. Introduce the first tracking error as

$$e_1 = x_{1d} - x_1 \qquad (14)$$

The first Lyapunov function is chosen as

$$V_1(e_1) = \frac{1}{2}e_1^2 \qquad (15)$$

the derivative of V_1 with respect to time is

$$\dot{V}_1(e_1) = e_1\dot{e}_1 = e_1(\dot{x}_{1d} - \dot{x}_1) \qquad (16)$$

For the purpose of stabilizing e_1, a stabilizing function is designed as

$$\alpha_1 = \dot{x}_{1d} + k_1 e_1 \qquad (17)$$

Substituting $\dot{x}_1$ by Equation (17), then the Equation (16) can be rewritten as

$$\dot{V}_1(e_1) = e_1(\dot{x}_{1d} - \dot{x}_{1d} - k_1 e_1) = -k_1 e_1^2 \leq 0 \quad (18)$$

where the parameter k_1 is a positive constant.

Step 2. The deviation of α_1 from the desired value $\dot{x}_1$ can be defined as the second tracking error

$$e_2 = \dot{x}_1 - \alpha_1 = \dot{x}_1 - \dot{x}_{1d} - k_1 e_1 \qquad (19)$$

the derivative of e_2 can be represented as

$$\dot{e}_2 = \ddot{x}_1 - \dot{\alpha}_1 = f(x_1) + g(x_{11})U_1 - \ddot{x}_{1d} - k_1 \dot{e}_1 \quad (20)$$

The second Lyapunov function is selected as

$$V_2(e_1, e_2) = \frac{1}{2}(e_1^2 + e_2^2) \qquad (21)$$

the derivative of V_2 with respect to time is

$$\dot{V}_2(e_1, e_2) = e_1\dot{e}_1 + e_2\dot{e}_2$$

$$\begin{aligned} &= e_1(\dot{x}_{1d} - \dot{x}_1) + e_2(\ddot{x}_1 - \dot{\alpha}_1) \\ &= e_1(-e_2 - k_1 e_1) + e_2(f(x_1) + g(x_{11}) \\ &\quad \times U_1 - \ddot{x}_{1d} - k_1\dot{e}_1) \\ &= -k_1 e_1^2 + e_2(-e_1 + f(x_1) + g(x_{11}) \\ &\quad \times U_1 - \ddot{x}_{1d} - k_1\dot{e}_1) \end{aligned} \qquad (22)$$

Step 3. For the purpose of stabilizing e_2, the control law U_1 is given as

$$U_1 = \frac{1}{g(x_{11})}(e_1 - f(x_1) + \ddot{x}_{1d} + k_1\dot{e}_1 - k_2 e_2) \quad (23)$$

where parameter k_2 is a positive constant. $C_\phi > 0, C_\theta > 0$ according to Assumption 4 and $m > 0$, so the $g(x_{11})$ is nonzero. Substituting (23) into (22), the derivative of V_2 can be rewritten as

$$\dot{V}_2(e_1, e_2) = -k_1 e_1^2 - k_2 e_2^2 \leq 0 \qquad (24)$$

namely $\dot{V}_2(e_1, e_2)$ is negative semi-definite. According to Lyapunov stability theory, the nonlinear system of quadrotor with Equation (8) is asymptotically stabilized using the control law (23). The designs of the other control inputs are similar to U_1.

4. Saturation integral backstepping control for the quadrotor UAV

The quadrotor UAV would be affected by some unpredictable external disturbance in actual application. Three different kinds of disturbances (constant disturbance, periodic disturbance and random disturbance) have been taken into account as the key disturbances in this section. The CBC method could hardly resist these external disturbances. Therefore, some effective auxiliary control is necessary to eliminate the effect on the quadrotor flight from the external disturbances. In this section, the saturation function and the integral of error are introduced into CBC to enhance its control robustness. With the external disturbance being taken into consideration, the nonlinear dynamic Equation (8) should be rewritten as

$$\ddot{\boldsymbol{X}} = f(\boldsymbol{X}) + g(\boldsymbol{X})\boldsymbol{U} + \boldsymbol{\delta} \qquad (25)$$

where $\boldsymbol{\delta} = \begin{bmatrix} \delta_1 & \delta_2 & \delta_3 & \delta_4 & \delta_5 & \delta_6 \end{bmatrix}^T$ is defined as the external disturbance vector, and the bound of the disturbance is $|\delta_i| \leq \beta(i = 1 \sim 6)$, while β is a given positive constant.

Taking U_1 as an example again and the design process of CBC and the reference [24] for reference. The design of SIBC is given step-by-step as follows:

Step 1. Introducing the first tracking error as

$$e_1 = x_{1d} - x_1 \qquad (26)$$

A new error variable (the integral of error e_1) is defined as

$$p_1 = \int_0^t e_1(\tau)\mathrm{d}\tau \qquad (27)$$

The first Lyapunov function is chosen as

$$V_1(p_1, e_1) = \frac{1}{2}\lambda_1 p_1^2 + \frac{1}{2}e_1^2 \qquad (28)$$

where λ_1 is a parameter of integral and the derivative of V_1 with respect to time is

$$\dot{V}_1(p_1, e_1) = \lambda_1 p_1 \dot{p}_1 + e_1 \dot{e}_1 = e_1(\dot{x}_{1d} - \dot{x}_1 + \lambda_1 p_1) \qquad (29)$$

A new stabilizing function is designed as

$$\alpha_1 = \dot{x}_{1d} + k_1 e_1 + \lambda_1 p_1 \qquad (30)$$

where the parameter k_1 is a positive constant.

Step 2. The second tracking error is defined as

$$e_2 = \alpha_1 - \dot{x}_1 = \dot{x}_{1d} - \dot{x}_1 + k_1 e_1 + \lambda_1 p_1 \qquad (31)$$

The derivative of e_2 can be represented as

$$\dot{e}_2 = \dot{\alpha}_1 - \ddot{x}_1 = \ddot{x}_{1d} - \ddot{x}_1 + k_1 \dot{e}_1 + \lambda_1 \dot{p}_1 \qquad (32)$$

Taking (31) into (29), $\dot{V}_1(p_1, e_1)$ is

$$\dot{V}_1(p_1, e_1) = -k_1 e_1^2 + e_1 e_2 \qquad (33)$$

The second Lyapunov function is selected as

$$V_2(p_1, e_1, e_2) = \frac{1}{2}\lambda_1 p_1^2 + \frac{1}{2}e_1^2 + \frac{1}{2}e_2^2 \qquad (34)$$

The derivative of V_2 with respect to time is

$$\begin{aligned}
\dot{V}_2(p_1, e_1, e_2) &= \dot{V}_1(p_1, e_1) + e_2 \dot{e}_2 \\
&= -k_1 e_1^2 + e_2(e_1 + \dot{e}_2) \\
&= -k_1 e_1^2 + e_2(e_1 + \ddot{x}_{1d} - \ddot{x}_1 \\
&\quad + k_1 \dot{e}_1 + \lambda_1 \dot{p}_1) \\
&= -k_1 e_1^2 + e_2((1 + \lambda_1 - k_1^2)e_1 + k_1 e_2 \\
&\quad - k_1 \lambda_1 p_1 + \ddot{x}_{1d} - f(x_1) \\
&\quad - g(x_{11})U_1 - \delta_1)
\end{aligned} \qquad (35)$$

In order to restrain the uncertain disturbance and stabilize the system, the control law U_1 can be designed as

$$U_1 = \frac{1}{g(x_{11})}((1 + \lambda_1 - k_1^2)e_1 + (k_1 + k_2)e_2 - k_1 \lambda_1 p_1$$
$$- \varepsilon_1 sat(e_2/\mu_1) + \ddot{x}_{1d} - f(x_1)) \qquad (36)$$

where the parameter k_2 is a positive constant, ε_1 is a design parameter, and the saturation function $sat(e_2/\mu_1)$ is defined as follows:

$$sat(e_2/\mu_1) = \begin{cases} 1 & e_2/\mu_1 > 1 \\ -1 & e_2/\mu_1 < -1 \\ e_2/\mu_1 & |e_2/\mu_1| \leq 1 \end{cases} \qquad (37)$$

Theorem 4.1: *Considering Assumptions 1–4, if the system error is controlled by the control law Equation (36), the solutions to the nonlinear dynamic system of quadrotor using Equation (25) will be uniformly ultimately bounded.*

Proof: substituting (36) into (35), the derivative of V_2 can be rewritten as

$$\dot{V}_2 = -k_1 e_1^2 - k_2 e_2^2 + e_2(\varepsilon_1 sat(e_2/\mu_1) + \delta_1) \qquad (38)$$

where δ_1 is bounded, let $A = \varepsilon_1 sat(e_2/\mu_1)$, A is bounded. Equation (38) can be represented as

$$\dot{V}_2 = -k_1 e_1^2 - k_2 e_2^2 + e_2 A + e_2 \delta_1 \qquad (39)$$

∎

The inequalities below are used here,

$$e_2 A \leq \frac{1}{2\gamma_1}e_2^2 + \frac{\gamma_1}{2}A^2 \qquad (40)$$

$$e_2 \delta_1 \leq \frac{1}{2\gamma_2}e_2^2 + \frac{\gamma_2}{2}\delta_1^2 \qquad (41)$$

where γ_1, γ_2 are positive constants, and Equation (39) can be obtained as

$$\begin{aligned}
\dot{V}_2 &\leq -2k_1 \frac{e_1^2}{2} - 2\left(k_2 - \frac{1}{2\gamma_1} - \frac{1}{2\gamma_2}\right)\frac{e_2^2}{2} \\
&\quad + \frac{\gamma_1}{2}A^2 + \frac{\gamma_2}{2}\delta_1^2
\end{aligned} \qquad (42)$$

Let $c = \min\{2k_1, 2(k_2 - (1/2\gamma_1) - (1/2\gamma_2))\}$, $d = (\gamma_1/2)A^2 + (\gamma_2/2)\delta_1^2$, where $k_1 > 0$ and $k_2 > (1/2\gamma_1) + (1/2\gamma_2)$, $\dot{V}_2$ can be rewritten as

$$\dot{V}_2 \leq -c\frac{e_1^2 + e_2^2}{2} + d = -cV + d \qquad (43)$$

which implies

$$V_2 \leq \left(V(t_0) - \frac{d}{c}\right)e^{-c(t-t_0)} + \frac{d}{c} \qquad (44)$$

According to the uniformly ultimately bounded theorem of the nonvanishing perturbation [25,26], the errors e_1 and e_2 of system are uniformly ultimately bounded.

The designs of the other control inputs are similar to U_1. Altogether, the control inputs U_1, U_2, U_3, U_4 and the virtual control inputs u_x and u_y for the quadrotor nonlinear system can be formulated as follows:

$$U_1 = \frac{1}{g(x_{11})}((1 + \lambda_1 - k_1^2)e_1 + (k_1 + k_2)e_2$$
$$- k_1 \lambda_1 p_1 - \varepsilon_1 sat(e_2/\mu_1) + \ddot{x}_{1d} - f(x_1))$$

$$U_2 = \frac{1}{g(x_{22})}((1 + \lambda_2 - k_3^2)e_3 + (k_3 + k_4)e_4$$
$$- k_3 \lambda_2 p_2 - \varepsilon_2 sat(e_4/\mu_2) + \ddot{x}_{2d} - f(x_2))$$

$$U_3 = \frac{1}{g(x_{33})}((1 + \lambda_3 - k_5^2)e_5 + (k_5 + k_6)e_6$$

$$-k_5\lambda_3 p_3 - \varepsilon_3 sat(e_6/\mu_3) + \dddot{x}_{3d} - f(x_3))$$

$$U_4 = \frac{1}{g(x_{44})}((1 + \lambda_4 - k_7^2)e_7 + (k_7 + k_8)e_8$$

$$-k_7\lambda_4 p_4 - \varepsilon_4 sat(e_8/\mu_4) + \dddot{x}_{4d} - f(x_4))$$

$$u_x = \frac{m}{U_1}((1 + \lambda_5 - k_9^2)e_9 + (k_9 + k_{10})e_{10}$$

$$-k_9\lambda_5 p_5 - \varepsilon_5 sat(e_{10}/\mu_5) + \dddot{x}_{5d} - f(x_5))$$

$$u_y = \frac{m}{U_1}((1 + \lambda_6 - k_{11}^2)e_{11} + (k_{11} + k_{12})e_{12}$$

$$-k_{11}\lambda_6 p_6 - \varepsilon_6 sat(e_{12}/\mu_6) + \dddot{x}_{6d} - f(x_6)) \quad (45)$$

Remark 4.1: The design process and uniformly ultimately boundedness proving process of the attitude controllers U_2, U_3, U_4 and virtual control inputs u_x, u_y are similar to those of U_1. u_x and u_y which were derived from Equation (45) and are substituted into Equation (11) to achieve the desired value ϕ_d and θ_d of the roll angle ϕ and the pitch angle θ. ϕ_d and θ_d which used as the control inputs of U_2 and U_3 are described as

$$\phi_d = x_{2d} = \arcsin(u_x \sin(\psi) - u_y \cos(\psi))$$

$$\theta_d = x_{3d} = \arcsin\left(\frac{u_x - \sin(\theta)\sin(\psi)}{\cos(\theta)\cos(\psi)}\right) \quad (46)$$

The quadrotor control scheme is shown in Figure 3.

5. Simulation results

In this section, in order to validate the designed SIBC strategy, simulations in two cases (hovering and trajectory tracking) are carried out by MATLAB/SIMULINK, with three kinds of external disturbances (constant disturbance, periodic disturbance and random disturbance) taken into consideration.

The model parameters of the quadrotor [27] used in simulation are modified as: $m = 0.65$ kg, $g = 9.81$ m/s^2, $l = 0.27$ m, $I_x = I_y = 0.0051$ kgm^2, $I_z = 0.0076$ kgm^2, $J_r = 2.8385 \times 10^{-5}$ kgm^2, $b = 2.9842 \times 10^{-6}$ Ns^2, $d = 3.232 \times 10^{-7}$ Nms^2. The control parameters are

chosen as $k_1 = k_2 = 3$, $k_3 = k_4 = 1$, $k_5 = k_6 = 2$, $k_7 = k_8 = k_9 = k_{10} = 10$, $k_{11} = k_{12} = 5$, $\gamma_1 = \gamma_2 = 2$, $\lambda_1 = \lambda_2 = 5$, $\lambda_3 = 3$, $\lambda_4 = \lambda_5 = 8$, $\lambda_6 = 5$, $\mu_1 = \mu_2 = 1$, $\mu_3 = 0.6$, $\mu_4 = \mu_5 = 0.5$, $\mu_6 = 0.4$, $\epsilon_1 = 4$, $\epsilon_2 = 6$, $\epsilon_3 = 5$, $\epsilon_4 = \epsilon_5 = 1$, $\epsilon_6 = 3$.

5.1. Case 1: hovering problem

In the hovering simulation, the desired value of position and attitude is given by $X_d = \begin{bmatrix} \psi_d & z_d & x_d & y_d \end{bmatrix}^T = \begin{bmatrix} 0 & 1 & 0.6 & 0.8 \end{bmatrix}^T$, the initial value are given as $\psi = 0$, $z = 1$, $x = 0.6$, $y = 0.8$, namely, the quadrotor will remain hovering at the desired position. The simulation is conducted based on 4-order Runge–Kutta method with the sampling time fixed on $\Delta t = 0.01$s, and the simulation time is given as $t = 20$ s. Two different external disturbances are applied from the 6th second on. Firstly, constant disturbance is given as $f_x = 2N$, $f_y = 1N$, $f_z = 2N$ and $M_x = M_y = M_z = 0.05$Nm, where f_x, f_y and f_z are the disturbing forces, and M_x, M_y and M_z are the disturbing torques. Secondly, periodic disturbance is given as $f_x = f_y = f_z = 0.5 \times \sin(t)N$, and $M_x = M_y = M_z = 0.1 \times \sin(t)$Nm. Simulation results are shown in Figures 4 and 5. The control inputs under periodic disturbance are shown in Figures 6 and 7.

The simulation results show that the quadrotor can keep hovering with CBC, IBC and SIBC strategy from 0 to 6 s as shown in Figures 4 and 5. However, after the addition of constant disturbance from the 6th second on, the quadrotor could not keep hovering with CBC strategy at the original position. The IBC or SIBC was able to restore the quadrotor hovering at the original position after a few seconds, although some vibration occurred as the constant disturbance was added into the system. In addition the amplitude and the restore time using SIBC are much smaller than those using IBC as shown in Figure 4(a–d). Figure 4(e) and (f) show the change of roll and pitch using the three control strategies. When the periodic disturbance was added at the 6th second, the position and yaw of UAV have shown a certain vibration relative to the initial value. However, the amplitude using SIBC is much smaller than those using CBC and IBC, which indicates that SIBC can keep
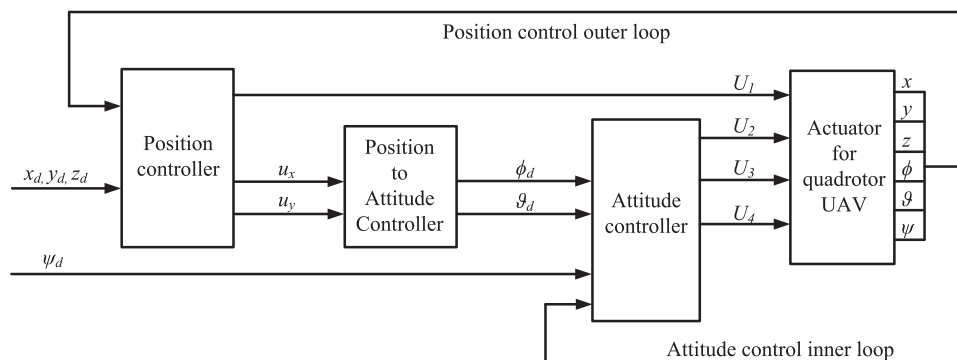
Figure 3. Block diagram of quadrotor control scheme.
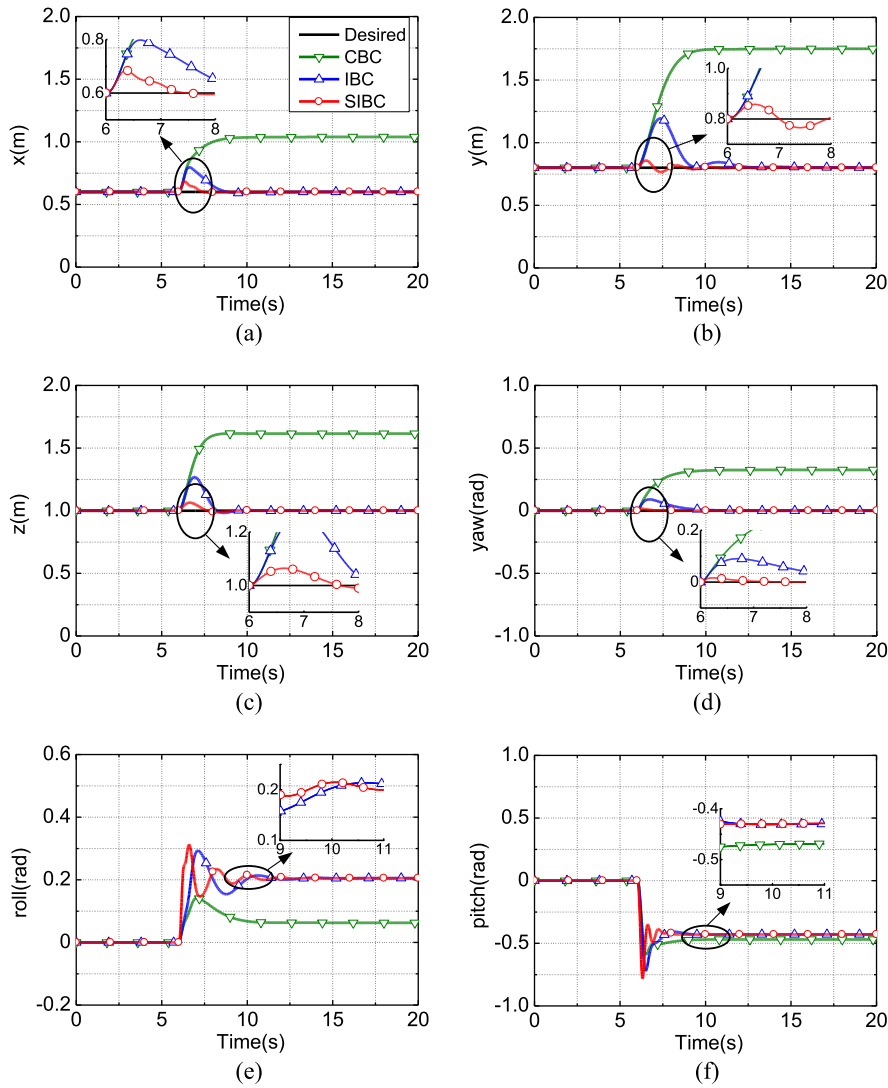
Figure 4. Analysis of the hovering using CBC, IBC or SIBC under the constant disturbance.

quadrotor hovering more stable than either one of the other two control strategies as shown in Figure 5(a–d).

Therefore, the SIBC strategy shows a better performance of the disturbance restraint in the hovering condition compared to the other two control strategies. Figures 6 and 7 show the control inputs of the three control strategies under two different external disturbances, respectively.

5.2. Case 2: trajectory tracking problem

In the trajectory tracking simulation, the control objective is to ensure that the quadrotor can track the desired trajectory which is adopted by the helical trajectory. The desired trajectory is described as

$$\begin{cases} x_d &= \sin(t) \\ y_d &= \sin(t) \\ z_d &= 0.5 + 0.3t \\ \psi_d &= 0 \end{cases} \tag{47}$$

The initial values are given as $\psi = 0$, $z = 0.5$, $x = 0$, $y = 1$. The simulation is conducted based on 4-order Runge–Kutta method with sampling time fixed on $\Delta t = 0.01$s, and the simulation time is 30 s. Three different external disturbances are given from 0th second on. Firstly, the constant disturbance is given as $f_x = f_y = f_z = 0.5$N and $M_x = M_y = M_z = 0.1$Nm, where f_x, f_y and f_z are the disturbing forces, and M_x, M_y and M_z are the disturbing torques. Secondly, the periodic disturbance is given as $f_x = f_y = f_z = 0.3 \times \sin(t)$N and $M_x = M_y = M_z = 0.05 \times \sin(t)$Nm. Thirdly, the random disturbance is given as $f_x = f_y = f_z = (0.5 \times e^{-0.1t} \sin(t) + \sigma_1)$N and $M_x = M_y = M_z = (0.1 \times e^{-0.1t} \sin(t) + \sigma_2)$Nm, where σ_1 and σ_2 are random numbers, with $|\sigma_1| \leq 2$, and $|\sigma_2| \leq 1$. Simulation results are shown in Figures 8–10. The tracking errors under constant disturbance, periodic disturbance and random disturbance using the three control strategies are shown in Figures 11–13.

As shown in Figures 8(a), 9(a), 10(a), 8(b), 9(b) and 10(b), the tracking results using the CBC and IBC strategies produced large constant error, periodic error
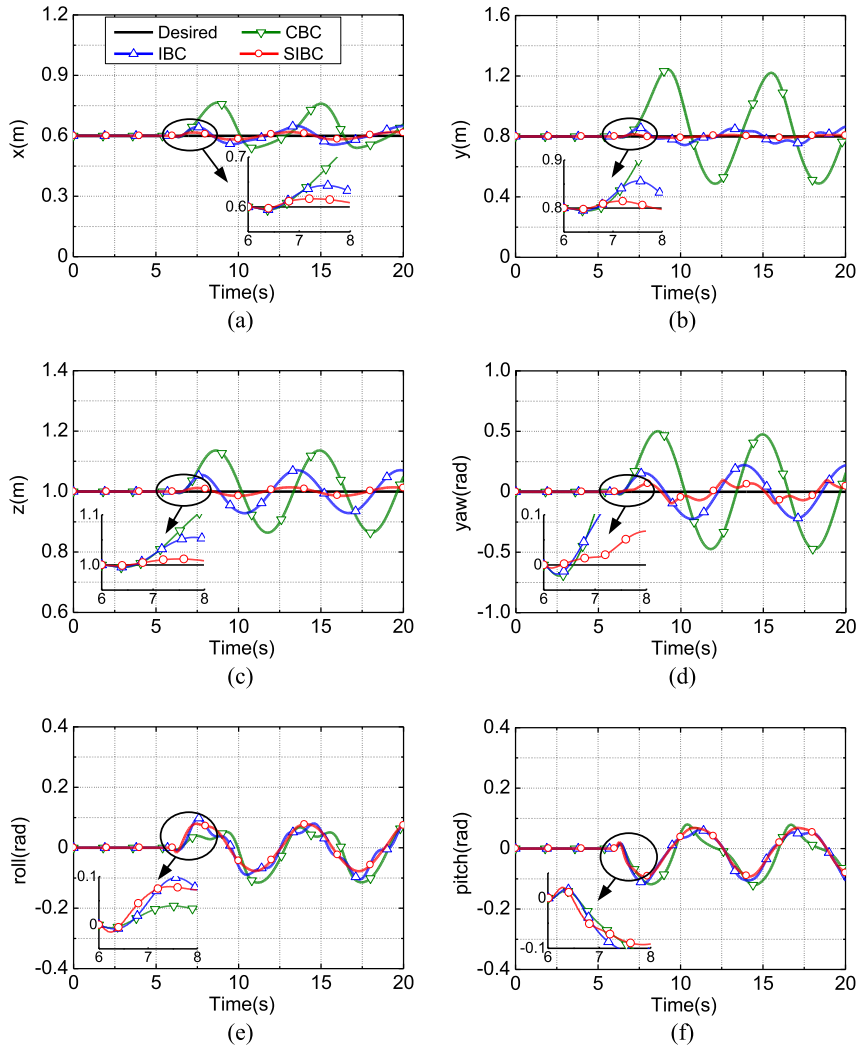
Figure 5. Analysis of the hovering using CBC, IBC or SIBC under the periodic disturbance.
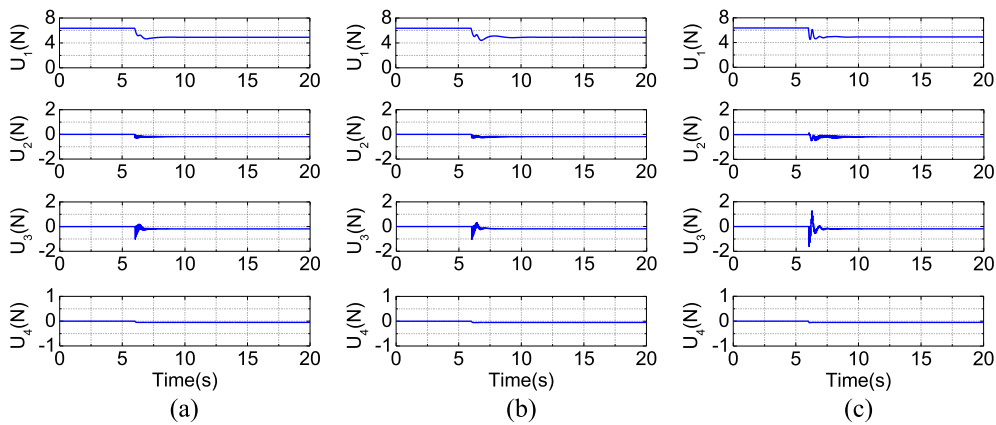
Figure 6. Control inputs of the hovering under the constant disturbance, (a)–CBC; (b)–IBC; (c)–SIBC.

and random error under the constant disturbance, periodic disturbance and random disturbance situations, respectively. These demonstrate that the CBC and IBC strategies exhibits weak disturbance restraint to trajectory tracking under the above three disturbances. In contrast the errors for the three disturbances convergence rapidly and stay stable within a small region after a transitory fluctuation respectively using the SIBC

strategy as shown in Figures 8(c), 9(c) and 10(c). The results indicate that the addition of saturation function and integral of tracking error into the original control laws can remarkably restrain the above disturbances respectively with a relatively high tracking accuracy.

Form Figures 11–13, the tracking errors of x, y, z and ψ are much smaller using SIBC under the three
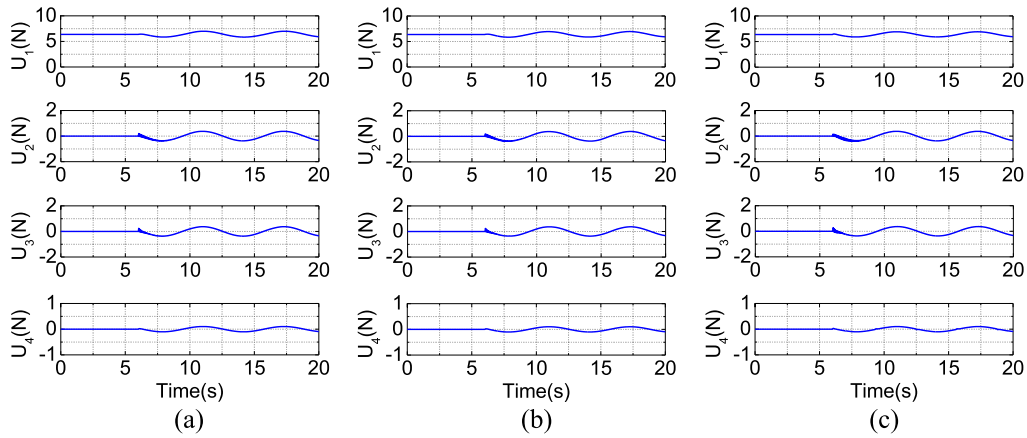
Figure 7. Control inputs of the hovering under the periodic disturbance, (a)–CBC; (b)–IBC; (c)–SIBC.
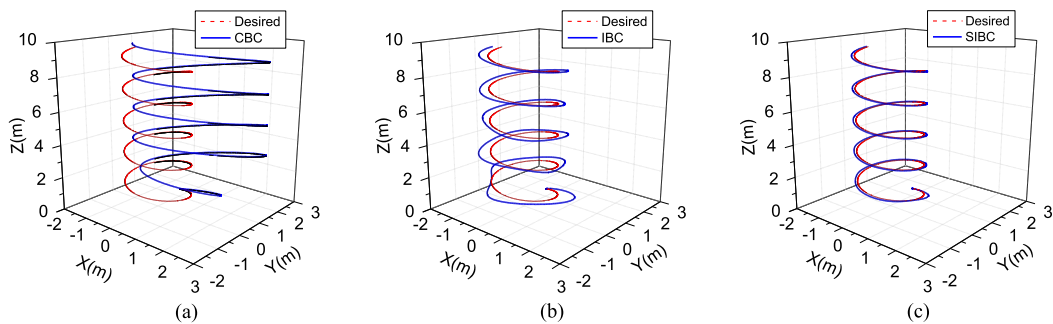
Figure 8. The trajectory tracking under constant disturbance. (a)–CBC; (b)–IBC; (c)–SIBC.
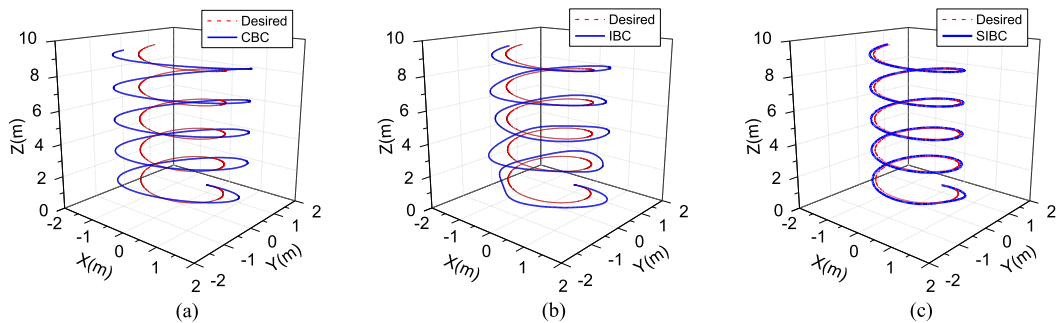
Figure 9. The trajectory tracking under periodic disturbance. (a)–CBC; (b)–IBC; (c)–SIBC.
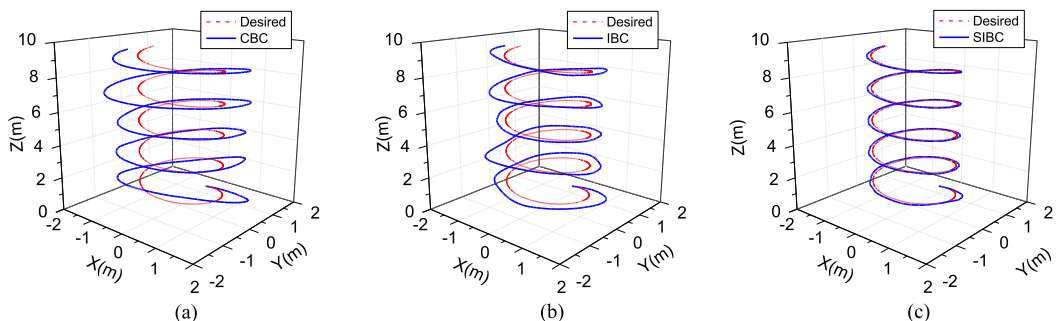
Figure 10. The trajectory tracking under random disturbance. (a)–CBC; (b)–IBC; (c)–SIBC.

disturbances than those using CBC or IBC (decreasing 30% to 80%). The roll and pitch using CBC, IBC and SIBC under the three disturbances are shown in Figures 14–16.

6. Experimental results

In order to illustrate the effectiveness of the proposed SIBC strategy, a series of trajectory tracking experiments of quadrotor UAV under the random
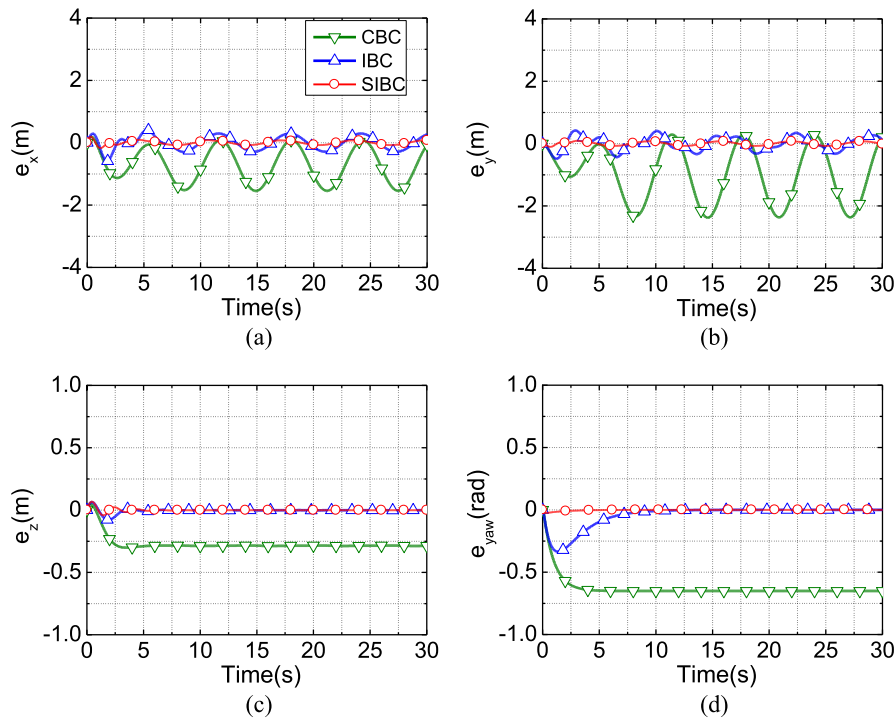
Figure 11. The tracking errors under constant disturbance using CBC, IBC or SIBC.
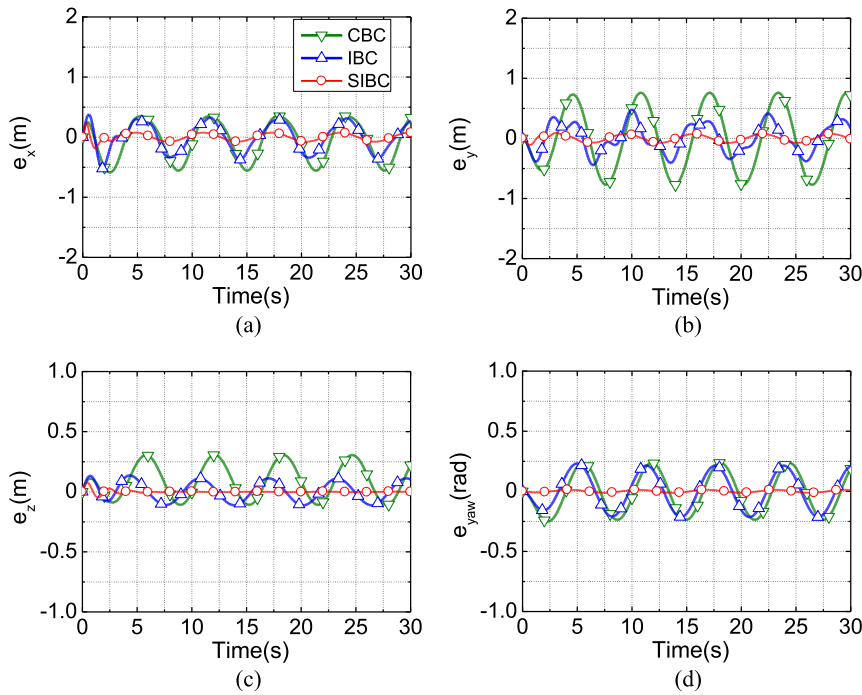
Figure 12. The tracking errors under periodic disturbance using CBC, IBC or SIBC.

disturbance from wind outdoors are presented in this section.

6.1. Experimental equipments

The actual experimental equipments of quadrotor UAV are shown in Figure 17. The main processor is STM32F407 (1M FLASH, 192K RAM, operates at 168 MHz) which is employed to control the propulsion system by PWM signals. A 12-Channel 2.4 GHz remote control system RadioLink-AT10 is used to keep communication with the main processor. The sensors (including ICM-20602, barometric pressure sensor SPL06 and 3-axis electronic compass AK8975) are utilized to measure the accelerations and angular rates in three directions, the altitude and the course angle, respectively. The relative height and the horizontal position of quadrotor UAV are measured by laser radar
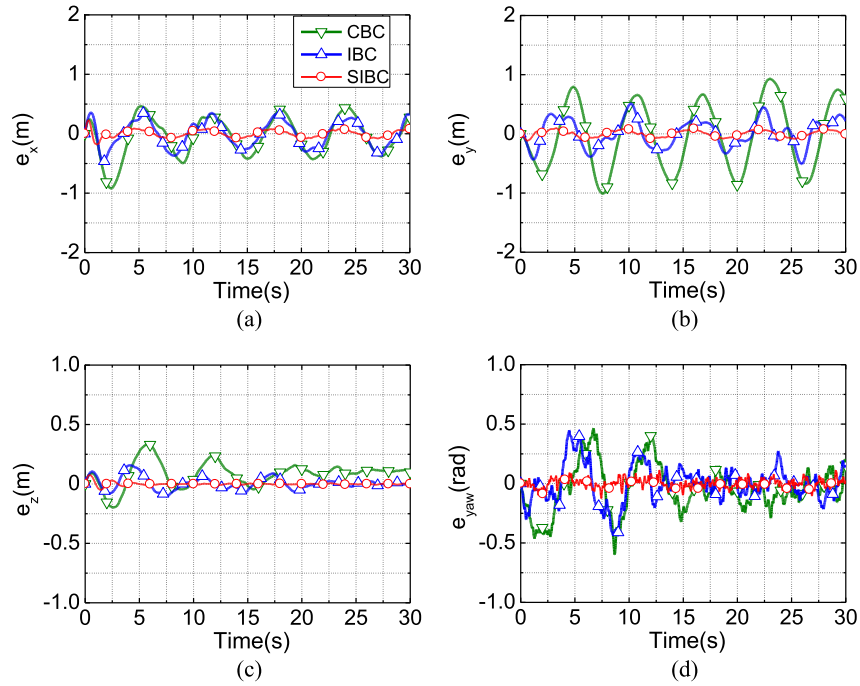
Figure 13. The tracking errors under random disturbance using CBC, IBC or SIBC.
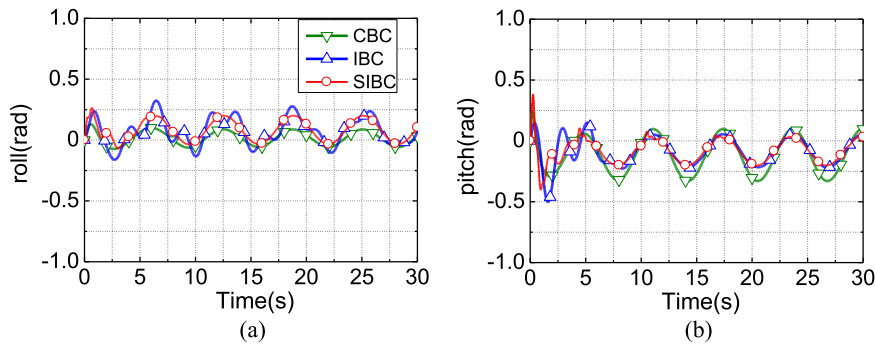
Figure 14. The roll and pitch under constant disturbance using CBC, IBC or SIBC.
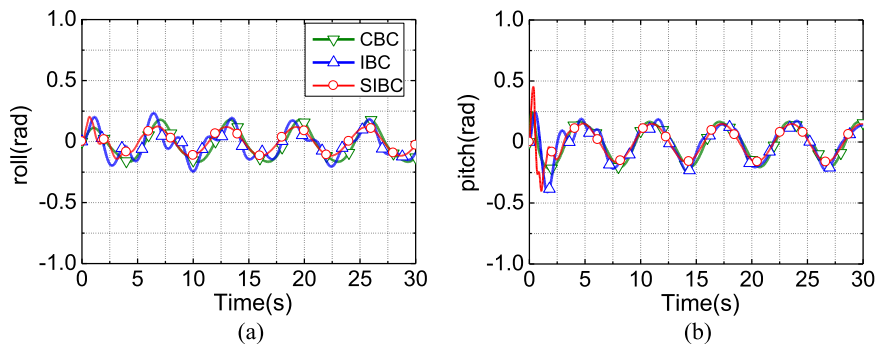
Figure 15. The roll and pitch under periodic disturbance using CBC, IBC or SIBC.

TFmini and Ultra Wideband (UWB), respectively. The quadrotor UAV powered by a 2600 mAh LI-Po battery can keep flying for 10–15 mins.

6.2. Flight experimental results and analysis

The trajectory tracking experiment of quadrotor UAV outdoors is shown in Figure 18. The outdoor temperature was 2°C, and the speed of the wind was around $1 \sim 2$ m/s with uncertain wind direction. The desired

trajectory on the x-y plane is described as $x_d - y_d = 0$, the desired value on z-axis is $z_d = 1.5$m, and the initial value are $x(0) = y(0) = 1$m, $z(0) = 1.5$m. The flight time is 10 s.

As shown in Figure 18, the UWB distance detection operates at Tri-anchors model, in which the three anchors are vertically placed with the distance between anchor 0–1 and 0–2 both being 3 m. The experimental results using CBC, IBC and SIBC are shown in Figure 19. As shown in Figure 19(a) and (b), the
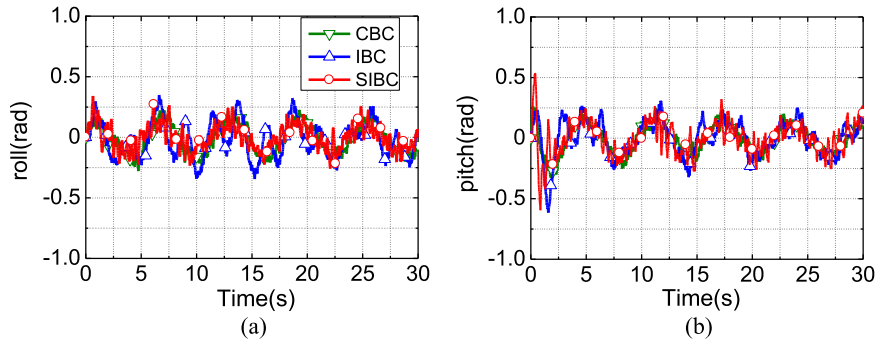
Figure 16. The roll and pitch under random disturbance using CBC, IBC or SIBC.

Figure 17. Experimental equipments of quadrotor UAV.
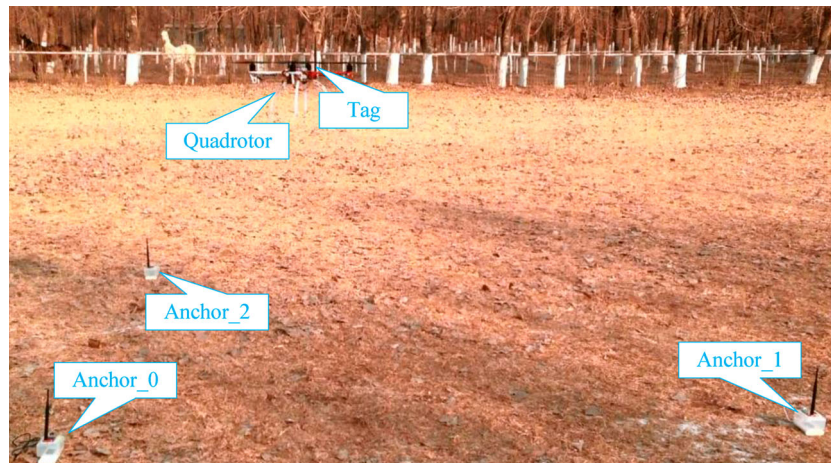
Figure 18. The trajectory tracking flight experiment of quadrotor UAV.

trajectories on x-y plane and z-axis using SIBC are in accordance with the desired trajectories with higher goodness of fit compared with those using CBC and IBC. In addition, the root mean square (RMS) errors of trajectory using CBC, IBC and SIBC are 1.14, 0.47 and 0.24 m, respectively, which indicates the RMS errors using SIBC is obviously smaller than those using CBC and IBC with the RMS errors reduced about $50 \sim 80\%$.

The flight experiment results are in accordance with the simulation results in Section 5, which further confirmed that the SIBC strategy can restrain the uncertain external disturbances more effectively than the other
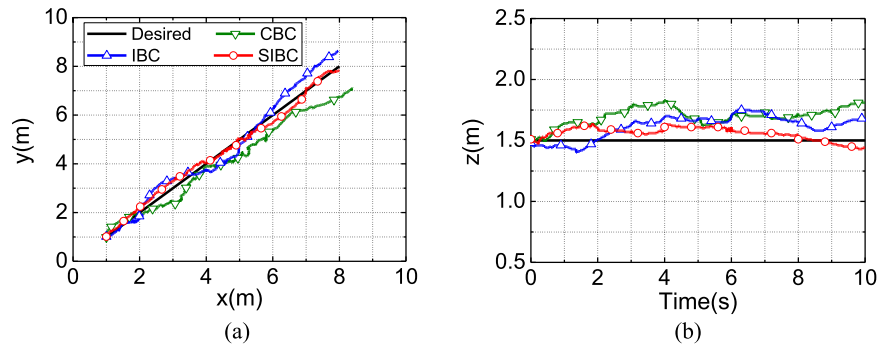
Figure 19. Experimental results of the trajectory tracking using CBC, IBC or SIBC.

two control strategies, and it will be a valuable control method in quadrotor UAV control field.

7. Conclusions

In order to reduce the effect from different external disturbances on quadrotor which is a highly unstable nonlinear system in actual application, a novel nonlinear robust controller SIBC for quadrotor is presented in this work. By introducing saturation function and integral of error into CBC, the SIBC strategy can remarkable reduce the interference with quadrotor system from the external disturbances such as constant disturbance, periodic disturbance and random disturbance. The boundedness of the nonlinear system has been proved by the uniformly ultimately bounded theorem of the nonvanishing perturbation. The results of hovering and trajectory tracking simulation and experiment show that the anti-disturbance capacity of SIBC is much better than that of CBC and IBC, which means that the SIBC with an excellent robustness has a potential application as a novel control strategy in actual quadrotor flight.

Disclosure statement

No potential conflict of interest was reported by the authors.

ORCID

Laihong Zhou 🔘 http://orcid.org/0000-0002-3434-2848

References

[1] Samir B, Roland S. Full control of a quadrotor. In: Proceedings of the IEEE/RSJ International Conference on Intelligent Robots and Systems; San Diego, CA; 2007. p. 153–158.

[2] Choi YC, Ahn HS. Nonlinear control of quadrotor for point tracking: actual implementation and experimental tests. IEEE/ASME Trans Mechatron. 2015;20(3):1179–1192.

[3] Meng W, Hu YC, Lin J, et al. ROSUnitysim: development and experimentation of a real-time simulator for multi-unmanned aerial vehicle local planning. Simulation. 2016;92(10):931–944.

[4] Orsag M, Poropat M, Bogdan S. Hybrid fly-by-wire quadrotor controller. Automatika. 2010;51(1):19–32.

[5] Raffo GV, Ortega MG, Rubio FR. An underactuated H∞ control strategy for a quadrotor helicopter. In: Proceedings of the European Control Conference; Budapest, Hungary; 2009. p. 3845–3850.

[6] Raffo GV, Ortega MG, Rubio FR. An integral predictive/nonlinear H∞ control structure for a quadrotor helicopter. Automatika. 2010;46(1):29–39.

[7] Zuo Z. Trajectory tracking control design with command filtered compensation for a quadrotor. IET Control Theory Appl. 2010;4(11):2343–2355.

[8] Zemalache K, Tahar M, Benhadria MR. Fuzzy integral sliding mode based on backstepping control synthesis for an autonomous. Proc Inst Mech Eng G J Aerospace Eng. 2013;227(G5):751–765.

[9] Mokhtari A, Benallegue A, Orlov Y. Exact linearization and sliding mode observer for a quadrotor unmanned aerial vehicle. Int J Robot Autom. 2006;21(1):39–49.

[10] Altug E, Ostrowski JP, Mahony R. Control of a quadrotor helicopter using visual feedback. In: IEEE International Conference on Robotics and Automation; Washington; 2002. p. 72–77.

[11] Choi IH, Bang HC. Quadrotor-tracking controller design using adaptive dynamic feedback-linearization method. Proc Inst Mech Eng G J Aerospace Eng. 2014;228(12):2329–2342.

[12] Wang T, Xie WF, Zhang YM. Sliding mode reconfigurable control using information on the control effectiveness of actuators. J Aerospace Eng. 2014;27(3):587–596.

[13] Besnard L, Shtessel YB, Landrum B. Quadrotor vehicle control via sliding mode controller driven by sliding mode disturbance observer. J Frankl Inst. 2012;349(2):658–684.

[14] Ryan T, Kim HJ. LMI-based gain synthesis for simple robust quadrotor control. Autom Sci Eng IEEE Trans. 2013;10(4):1173–1178.

[15] Lee T. Robust adaptive attitude tracking onwith an application to a quadrotor UAV. IEEE Trans Control Syst Technol. 2013;21(5):1924–1930.

[16] Chamseddine A, Theilliol D, Zhang YM, et al. Active fault tolerant control system design with trajectory replanning against actuator faults and saturation: application to a quadrotor unmanned aerial vehicle. Int J Adapt Control Signal Process. 2015;29(1):1–23.

[17] Morel Y, Leonessa A. Direct adaptive tracking control of quadrotor aerial vehicles. In: Conference on Resent Advances in Robotics; Miami, Florida; 2006.

[18] Bouchoucha M, Tadjine M, Tayebi A, et al. Step by step robust nonlinear PI for attitude stabilisation of a four-rotor miniaircraft. In: Proceedings of the 16th Mediterranean Conference on Control and Automation; Ajaccio, France; 2008. p. 1276–1283.

[19] Basri MAM, Husain AR, Danapalasingam KA. Enhanced backstepping controller design with application to autonomous quadrotor unmanned aerial vehicle. J Intell Robotic Syst. 2015;79(2):295–321.

[20] Chen FY, Lei W, Zhang KK, et al. A novel nonlinear resilient control for a quadrotor UAV via backstepping control and nonlinear disturbance observer. Nonlinear Dyn. 2016;85(2):1281–1295.

[21] Wang C, Song B, Huang P, et al. Trajectory tracking control for quadrotor robot subject to payload variation and wind gust disturbance. J Intell Robotic Syst. 2016;83(2):315–333.

[22] Hoffmann GM, Huang H, Waslander SL, et al. Precision flight control for a multi-vehicle quadrotor helicopter testbed. Control Eng Pract. 2011;19(9): 1023–1036.

[23] Islam S, Liu PX, Saddik AE. Nonlinear adaptive control for quadrotor flying vehicle. Nonlinear Dyn. 2014;78(1):117–133.

[24] Fang Z, Gao W, Zhang L. Robust adaptive integral backstepping control of a 3-DOF helicopter. Int J Adv Rob Syst. 2012;9(5):637–647.

[25] Khalil HK. Nonlinear systems. Upper Saddle River (NJ): Prentice Hall; 1996.

[26] Li YX, Yang GH. Fuzzy adaptive output feedback fault-tolerant tracking control of a class of uncertain nonlinear systems with nonaffine nonlinear faults. IEEE Trans Fuzzy Syst. 2016;24(1):223–234.

[27] Derafa L, Madani T, Benallegue A. Dynamic modelling and experimental Identification of four rotors helicopter parameters. In: IEEE International Conference on Industrial Technology; IEEE; 2006. p. 1834–1839.